© 2023. Published by The Company of Biologists Ltd | Development (2023) 150, dev201464. doi:10.1242/dev.201464

RESEARCH ARTICLE

Molecular profiling of the vestibular lamina highlights a key role for Hedgehog signalling

Tengyang Qiu[1,2], Barbora Hutečková[3,4], Maisa Seppala[1,5], Martyn T. Cobourne[1,5], Zhi Chen[2], Mária Hovořáková[6], Marcela Buchtová[3,4] and Abigail S. Tucker[1,6,*]

ABSTRACT

The vestibular lamina (VL) forms the oral vestibule, creating a gap between the teeth, lips and cheeks. In a number of ciliopathies, formation of the vestibule is defective, leading to the creation of multiple frenula. In contrast to the neighbouring dental lamina, which forms the teeth, little is known about the genes that pattern the VL. Here, we establish a molecular signature for the usually non-odontogenic VL in mice and highlight several genes and signalling pathways that may play a role in its development. For one of these, the Sonic hedgehog (Shh) pathway, we show that co-receptors *Gas1*, *Cdon* and *Boc* are highly expressed in the VL and act to enhance the Shh signal from the forming incisor region. In *Gas1* mutant mice, expression of *Gli1* was disrupted and the VL epithelium failed to extend due to a loss of proliferation. This defect was exacerbated in *Boc*/*Gas1* double mutants and could be phenocopied using cyclopamine in culture. Signals from the forming teeth, therefore, control development of the VL, coordinating the development of the dentition and the oral cavity.

KEY WORDS: Vestibular lamina, Oral cavity, Sonic hedgehog, Gas1, Dental lamina, Ciliopathies, Mouse

INTRODUCTION

Odontogenesis proceeds through a series of characteristic stages, which are controlled by multiple molecular interactions between the epithelium and underlying mesenchyme. In mammals, the first sign of tooth development is the appearance of a band of thickened epithelium marked by the expression of *Pitx2* and *Shh* (Yu et al., 2020) This band goes on to form the dental lamina (DL), from which the tooth germs will emerge. Lateral to the DL is a second epithelial lamina, known as the vestibular lamina (VL) in mammals. In humans, the VL and DL have a complex relationship during early development, with the two laminas merging and branching as they run along the jaw margin (Hovorakova et al., 2005; 2007). In the anterior parts of the lower jaw, the DL and VL share a common origin, emerging from the same Shh-positive epithelial thickening in both mouse and human (Hovorakova et al., 2007, 2016; Qiu et al., 2020). As these structures diverge in development, Shh signalling is associated with the forming tooth germ, but turns off in the VL (Hovorakova et al., 2016). While the DL produces the teeth, the VL splits down the middle to form a space between the teeth and lips and teeth and cheeks, thereby creating the vestibule of the oral cavity. Given this role, the VL is also known as the labio-gingival ridge, lip-furrow band or cheek furrow ridge (Bolk, 1921; Schour, 1929; Peterková, 1985). During development, the lingual (tongue side) and buccal/labial (cheek/lip) sides of the VL are distinct in both mouse and human, with differences in rates of proliferation and expression of epithelial markers (Qiu et al., 2020; Qiu and Tucker, 2022). These differences may influence the opening of the lamina and they are later reflected by differences in molecular identity of the different parts of the oral mucosa.

The developing mammalian VL has a varied structure across mammals. In human and sheep, the VL is in general thick and wide, whereas in the vole and mouse, the VL is relatively thin and narrow (Pavlikova et al., 1999; Witter et al., 2005; Hovorakova et al., 2005, 2016; Qiu et al., 2020; Qiu and Tucker, 2022). The human VL is prominent throughout the upper and lower jaws and regionalized in parallel with the DL (Hovorakova et al., 2005, 2007). In contrast, the mouse only has a prominent VL in the anterior mandible, and the maxillary VL is almost absent (Qiu and Tucker, 2022). The relationship of the DL and VL also varies, with the DL branching off the VL in humans, while in mice both the DL and VL have a separate connection to the oral cavity. These differences are likely to correspond to the different morphologies of the vestibule and reflect differences in diet and chewing patterns.

A similar laterally situated lamina is also observed in reptiles. This lamina also appears to share a common origin with the adjacent DL. In the chameleon, this more lateral lamina develops into the dental glands that lubricate the teeth, while in poisonous snakes it forms the venom gland (Vonk et al., 2008; Tucker, 2010). It has been suggested that the mammalian VL and the reptilian dental gland lamina have evolved from laterally positioned DLs, similar to those that create the inner and outer dental arches in extant axolotls (Soukup et al., 2021) As the dentition became restricted to a single row of teeth in many tetrapods, the redundant DLs would have been lost or, in the case of the dental glands and VL, repurposed to create other ectodermal structures (Hovorakova et al., 2020).

Despite its shared origin with the DL, the VL does not normally form teeth. However, overexpression of Wnt signalling in the VL does lead to ectopic tooth formation in this structure in mice (Wang et al., 2009; Popa et al., 2019) and may explain the occasional occurrence of odontomas situated in the vestibule of human subjects (Hovorakova et al., 2020). Vestibular deficiencies have been

[1]Centre for Craniofacial & Regenerative Biology, Faculty of Dentistry, Oral & Craniofacial Sciences, King's College London, London, SE1 9RT United Kingdom. [2]The State Key Laboratory Breeding Base of Basic Science of Stomatology & Key Laboratory of Oral Biomedicine, Ministry of Education (Hubei-MOST KLOS & KLOBM), School and Hospital of Stomatology, Wuhan University, 430079 Wuhan, China. [3]Department of Experimental Biology, Faculty of Science, Masaryk University, 625 00 Brno, Czech Republic. [4]Laboratory of Molecular Morphogenesis, Institute of Animal Physiology and Genetics, Czech Academy of Sciences, 602 00 Brno, Czech Republic. [5]Department of Orthodontics, Faculty of Dentistry, Oral & Craniofacial Sciences, King's College London, London, SE1 9RT UK. [6]Institute of Histology and Embryology, First Faculty of Medicine, Charles University, Albertov 4, 128 00 Praha 2, Czech Republic.

*Author for correspondence (abigail.tucker@kcl.ac.uk)

M.T.C., 0000-0003-2857-0315; M.B., 0000-0002-0262-6774; A.S.T., 0000-0001-8871-6094

Handling Editor: Liz Robertson
Received 20 November 2022; Accepted 13 March 2023

Development (2023) 150, dev201464. doi:10.1242/dev.201464

reported in a number of human syndromes; in particular, in the ciliopathy Ellis-van Creveld (EvC) (MIM #225500), where development of the VL is defective, and the gums adhere to the upper lip and cheek with multiple associated frenula (Sasalawad et al., 2013). Recently, VL anomalies along with tooth abnormalities have also been observed in a patient with cryptophthalmos (MIM #123570) due to mutation in the *FREM2* gene (Kantaputra et al., 2022). In addition, a shallow (<4 mm) vestibule and frenula anomalies in the lower incisor region have been noted in a study of gingival phenotypes in healthy children (Kus-Bartoszek et al., 2022). Such deficiencies in frenulum attachment were suggested to be associated with certain periodontal diseases (Placek et al., 1974).

The stages of development of the VL have recently been characterized in mouse and human, with an analysis of proliferation, cell death and epithelial differentiation (Qiu and Tucker, 2022); however, no other data is available regarding the genes involved in shaping and directing the development of this structure. In addition, although the VL and the dentition share a common origin, whether these tissues interact during later development to coordinate oral development is unknown. To address this, a transcriptome of the murine VL at embryonic day (E) 14 was created to identify the molecular signature of this structure and compare it with the neighbouring cap stage incisor tooth germ. This allowed a comparison of odontogenetic and non-odontogenic tissue and identification of genes unique to the VL. At E14, the VL has extended into the lower jaw as a sheet of epithelium with higher proliferation on the labial and buccal sides away from the developing teeth (Qiu and Tucker, 2022). This suggested potential interactions between the tooth and VL. We, therefore, used the transcriptomic dataset to focus on signalling molecules expressed in the tooth and readouts in the VL to further understand how the two tissues might interact. Mouse mutants and explant culture were then used to test the function of identified pathways.

From this analysis, we identified previously unreported markers associated with the VL and highlighted Hedgehog (Hh) signalling from the developing tooth as playing a potential role in patterning the VL during development. Functional studies confirmed the role of Hh signalling in patterning the VL and demonstrated that signals from the tooth have a key role in orchestrating development of neighbouring structures, coordinating development of the teeth and the oral cavity.

RESULTS

A distinct molecular signature for the vestibular lamina at E14

The VL has odontogenic potential but does not normally form teeth (Popa et al., 2019). To identify the molecular signatures that distinguish the VL from the early tooth bud (TB) during development, we dissected the VL and TB from the incisor region of the murine mandible at E14 for analysis through bulk RNA-sequencing (RNA-seq) (Fig. 1A). At this stage, the anterior VL and incisor TB have developed their distinct morphologies and are clearly observed in sagittal slices, facilitating precise dissection. However, despite their morphological differences, the VL can still be induced to form tooth-like structures after stabilization of β-catenin at this late stage (Popa et al., 2019). Fate is, therefore, not yet determined in this structure at E14. The epithelium and mesenchyme were dissected together to provide a comprehensive characterization of the whole structure. The RNA-seq dataset included VL (n=5, VL1-5) and TB (n=5, TB1-5) samples, with the boxplot, violin plot and density plot showing consistent distributions of normalized read counts (counts per million; CPM) (Fig. S1A-C). A correlation plot confirmed that there was a higher correlation between the transcriptomic profile of VL-VL and TB-TB compared with TB-VL (Fig. S1D). Levels of vimentin (a general mesenchymal marker) and *Cdh1* (a general epithelial marker) were used to estimate the relative amounts of mesenchymal and epithelial tissue included in the analysis. No significant difference was observed in expression of these two markers between the TB and VL groups, suggesting that the dissected regions contained approximately equivalent numbers of mesenchymal and epithelial cells (Fig. S1E,F). Principal component analysis (PCA) presented distinct gene expression distributions between the VL and TB datasets at E14 (Fig. 1B). In total, 1788 differentially expressed genes (DEGs) were detected, including 788 upregulated (TB) and 1000 downregulated (VL) DEGs. The top DEGs were visualized by a volcano plot, where absolute value of log2 fold change (abs log2FC)>2 and P-value<0.01 (Fig. 1C). The DEGs were highlighted in a heatmap where abs log2FC>2 and P-value<0.001 (Fig. 1D). Overall, these results confirmed that the VL and TB were significantly different at the molecular level by E14. Our large-scale analysis of gene signatures confirmed that genes known to play a role in early tooth development were upregulated in the TB relative to the VL, including *Shh*, Fgfs, *Pax9*, Dlx homeobox gene-family members, *Runx2*, *Rspo1* and *Scube1* (Zhao et al., 2000; Seppala et al., 2007; Xavier et al., 2009; Kawasaki et al., 2014) (Fig. 1C,D), with gene expression patterns confirmed by RNAscope (Fig. S2). In addition, the screen highlighted a number of genes upregulated in the VL relative to the TB (Fig. 1C,D), with expression in the VL again confirmed by RNAscope (Fig. S3), or by checking expression on Genepaint (https://gp3.mpg.de/), a digital atlas highlighting gene expression in the embryo at E14.5 (Fig. S4) (Visel et al., 2004). These included *Meis1*/*2*, *Otx1* and *Nr4a2* transcription factors, and signalling pathway members *Cd44* and *Wnt7b*, which have not previously been associated with the VL. Interestingly, in keeping with the observed lingual-buccal/labial differences in the VL epithelium at this stage (Qiu and Tucker, 2022), some highlighted genes had clear lingual-buccal/labial differences in expression, such as *Otx1*, which was expressed on the labial side of the VL away from the tooth (Fig. S3L′). In addition, differential expression was evident in the oral and aboral parts of the VL, suggesting additional levels of compartmentalization (Fig. S4). Using this data, we were, therefore, able to create the first molecular signature for the VL.

Differential analysis highlights differences in Shh pathway component expression in the VL and TB

To understand how the tooth bud might impact on development of the VL, we focused on signalling pathways highlighted by the transcriptomics. As expected given its conserved role in tooth development, *Shh* was highlighted as differentially expressed in the tooth germ, along with patched 1 (*Ptch1*) and *Gli1* (Fig. 2A,B; Fig. S5A-F) (Buchtová et al., 2008; Seppala et al., 2017). *Ptch1* is a transmembrane domain protein that acts as the principal receptor for Shh, but also provides a readout of Shh signalling activity, whereas *Gli1* acts as a universal downstream transcriptional target. The Shh pathway is activated when *Shh* binds to *Ptch1*, which is facilitated by a number of co-receptors, including growth arrest-specific 1 (*Gas1*) and Ig/fibronectin subfamily transmembrane proteins *Boc* and *Cdon* (*Cdo*) (Tenzen et al., 2006; Seppala et al., 2022). *Gas1* is a vertebrate-specific glycosylphosphatidylinositol-anchored membrane protein proposed to be a co-receptor for Shh and positive regulator of the signal pathway in vertebrates (Martinelli and Fan, 2007; Seppala et al., 2022). In contrast to *Shh* and *Ptch1*, *Gas1*, *Cdon* and *Boc* were all significantly more

Development (2023) 150, dev201464. doi:10.1242/dev.201464

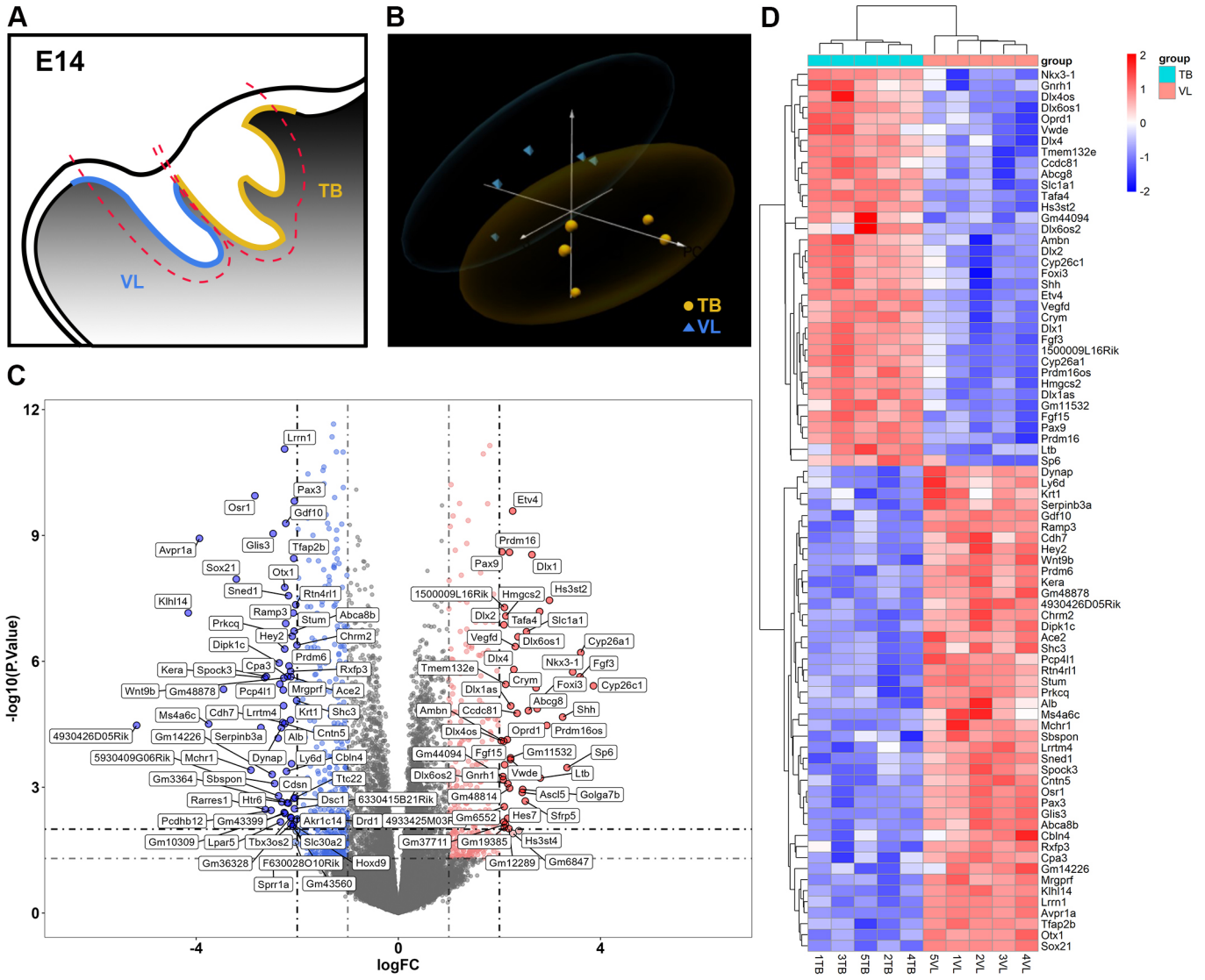

Fig. 1. Distinct gene signatures of the VL and TB at E14 revealed by RNA-seq. (A) Schematic of vestibular lamina (VL) and incisor tooth bud (TB) dissection for RNA-seq. Sagittal view. (B) PCA plot of the RNA-seq dataset for VL and TB samples. Blue and yellow dots represented VL and TB, respectively, in the scatterplot, with the ellipses showing clustering of the samples. Distinct gene expression distributions between the VL and TB were observed. (C) The volcano plot showed a number of upregulated (TB) and downregulated (VL) DEGs. Red represented selected highly expressed genes in TB, whereas blue emphasizes selected highly expressed genes in VL. Abs log2FC_1>1, *P*-value_1<0.05; abs log2FC_2>2, *P*-value_2<0.01. (D) Heatmap of signatures of VL and TB samples. A number of VL and TB markers were identified. Annotations show clustering of the samples. Abs log2FC>2 and *P*-value<0.001. The dissected VL and tooth germs from a single litter (9-15 embryos) were pooled to obtain enough RNA for sequencing. In total, tissue from 11 litters was isolated and pooled samples from five litters with the highest quality scores were used for analysis. These are referred to here as TB1-5 and VL1-5.

highly expressed in the VL (Fig. 2A,B). To further investigate the expression of these Shh pathway-related genes, we compared the expression of *Ptch1*, *Cdon*, *Shh*, *Gas1* and *Boc* in these two laminas at E12.5 (before obvious morphological differences in these structures) and at E15.5 (when the two structures are clearly morphologically distinct) (Fig. 2E-P). The VL runs as a continuous band anteriorly around the incisor tooth germs and, therefore, can be viewed both in sagittal plane for the labial lamina (Fig. 2C) and frontal plane for the buccal lamina (Fig. 2D). At E12.5, the VL (lined by green dashed line) and DL (lined by white dashed line) were evident as two side-by-side epithelial thickenings (Fig. 2E) with *Shh* expression restricted to the DL (Fig. 2H). *Ptch1* was expressed in the epithelium of the VL, DL and strongly in the surrounding mesenchyme (Fig. 2F). In contrast, expression of *Gas1* was mainly observed in the epithelium of the VL and the mesenchyme on the buccal side (Fig. 2I). *Cdon* and *Boc* showed similar expression patterns to *Gas1* (Fig. 2G,J). At E15.5, the VL curves as it extends into the mesenchyme so that it grows under the developing incisors and Meckel's cartilage, while the neighbouring incisor tooth germ has developed from a thickening to reach the late cap stage (Fig. 2K). At this stage, strong transcription of *Shh* was detected in the inner enamel epithelium of the incisors (Seppala et al., 2017); however, the adjacent VL was negative for *Shh* expression (Fig. 2N). *Ptch1* was highly expressed in the developing tooth, in the epithelium and surrounding mesenchyme, but relatively lower *Ptch1* expression was observed in the VL, mainly localized to the lower part of the VL (Fig. 2L). In contrast to the tooth germ-dominant expression of *Shh* and *Ptch1*, *Cdon*, *Gas1* and

Development (2023) 150, dev201464. doi:10.1242/dev.201464

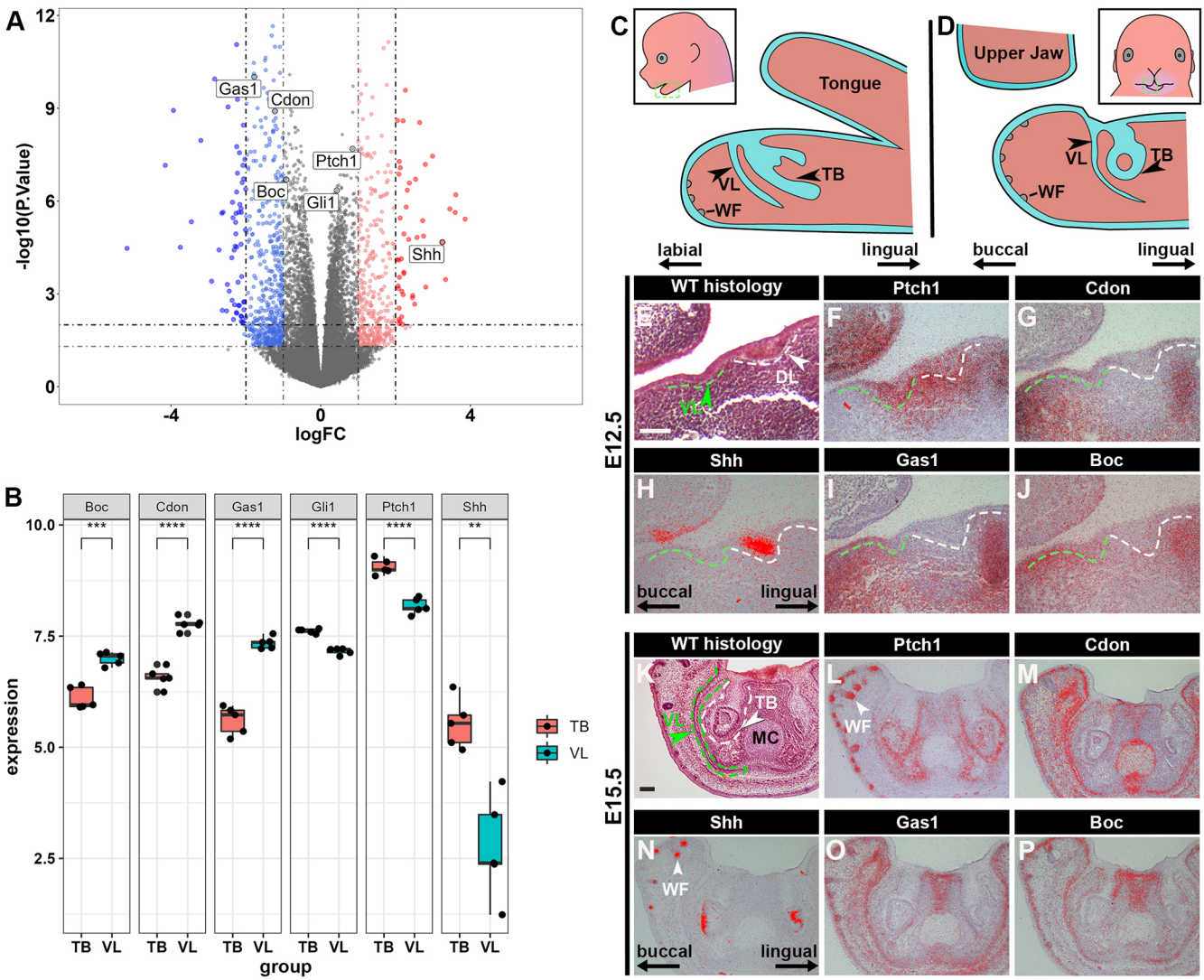

Fig. 2. Differential expression of Shh pathway components in the VL and tooth germ. (A,B) Volcano plot (A) and boxplot (B) highlighting the differences of Shh pathway-related genes in the vestibular lamina (VL) and incisor tooth germ at E14. *Gas1*, *Cdon* and *Boc* were significantly more highly expressed in the VL, whereas *Shh*, *Ptch1* and *Gli1* were significantly more highly expressed in the incisor tooth germ. Abs log2FC_1>1, *P*-value_1<0.05; abs log2FC_2>2, *P*-value_2<0.01. **P*<0.05, ***P*<0.01 and ****P*<0.001 (two-tailed, unpaired *t*-test). In box plots, middle bars represent median values, boxes represent first to third interquartile ranges and dots indicate the expression of each sample. (C) Schematic of E15.5 mouse lower jaw in the sagittal plane, showing the tooth bud (TB) and adjacent VL on the labial (lip) side of the TB. (D) Schematic of E15.5 mouse lower jaw in frontal plane, showing the TB and adjacent VL on the buccal (cheek) side of the TB. (E,K) Trichrome/H&E staining of the VL and dental lamina (DL)/tooth germ in the anterior lower jaw at E12.5 and E15.5. (F-J,L-P) Frontal sections of the lower jaw in the incisor region in WT (CD1) mouse performed with radioactive *in situ* hybridization. Shh pathway gene expression was assessed in the VL and DL/tooth bud/tooth germ at E12.5 and E15.5, respectively. (F,L) *Ptch1*; (G,M) *Cdon*; (H,N) *Shh*; (I,O) *Gas1*; (J,P) *Boc*. WF, whisker follicles; MC, Meckel's cartilage. Lingual-labial axes shown in C. Lingual-buccal axes shown in D,H,N, same plane for E-P. Scale bars: 100 µm.

Boc were reduced in the developing tooth germs but were strongly expressed on the buccal side of the VL in the buccal epithelium and mesenchyme (Fig. 2M,O,P). This buccal/labial bias of *Gas1* expression in the VL epithelium was confirmed at E14 by RNAscope (Fig. S5D-F).

Truncation of the VL in *Gas1* and *Boc* compound mutants

Given the distinct expression pattern of *Gas1* in the VL, we focused on this component of the Shh pathway through the analysis of *Gas1* mutant mice. *Gas1* has been shown to facilitate Shh signalling, particularly with low signal levels at long distance from the source (Martinelli and Fan, 2007). A lack of *Gas1* is associated with a series of midline craniofacial phenotypes including maxillary incisor fusion, midfacial hypoplasia and cleft palate due to reduced Shh signalling in the early craniofacial region (Seppala et al., 2007). At E13.5, the VL (contoured by green dashed lines) has started to extend into the mesenchyme under the forming incisors in wild-type (WT) mice, with full extension under the tooth germ, towards the midline, by E15.5 (Fig. 3A,F). In contrast, in the *Gas1* null mutants ($Gas1^{-/-}$), the VL was shorter and failed to pass under the forming incisors (Fig. 3B,G) (truncated VL observed in N=15/15 $Gas1^{-/-}$ embryos from E13.5 to E15.5). Interestingly, a similar truncated VL was observed in some $Gas1^{+/-}$ embryos at E13.5, although the severity of the defect varied between heterozygous mutants (Fig. 4J-L) (truncation observed in N=5/7 $Gas1^{+/-}$ embryos at E13.5). The reduction in the VL was significant in both homozygous and heterozygous mutants when measured at E13.5 (Fig. 4G).

Development (2023) 150, dev201464. doi:10.1242/dev.201464

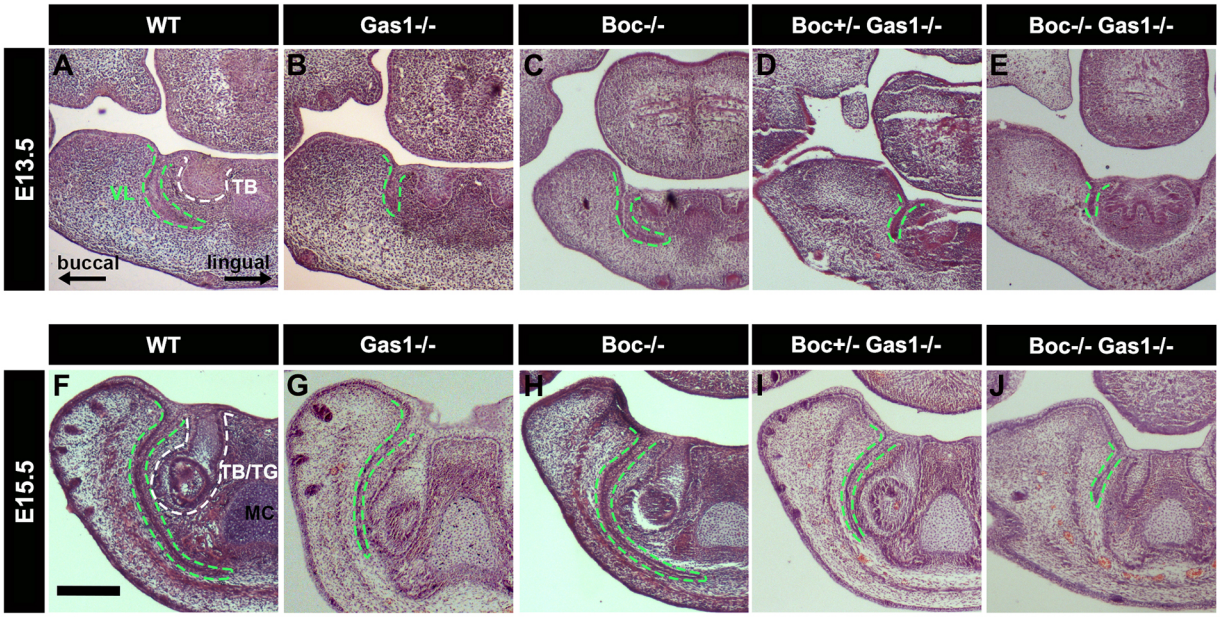

Fig. 3. Truncated VL formation after loss of Shh co-receptors. (A-J) Trichrome/H&E staining of mouse frontal sections through the lower incisor region. (A-E) E13.5. (A) In the WT, the vestibular lamina (VL) had extended into the mesenchyme and around the forming incisor tooth bud (TB). (B) *Gas1*$^{-/-}$. The mutant VL had started to extend but fails to pass the neighbouring incisor tooth bud. (C) *Boc*$^{-/-}$. Normal extension of the VL. (D) *Boc*$^{+/-}$*Gas1*$^{-/-}$. Defective extension. (E) *Boc*$^{-/-}$*Gas1*$^{-/-}$ compound mutant. The VL and tooth germs (TG) were severely affected, with a rudimentary VL and partial fusion of the incisors at the midline. (F-J) E15.5. (F) The WT VL at E15.5 had invaginated further into the mesenchyme and under Meckel's cartilage (MC) in the midline. (G) Similar to E13.5, the *Gas1*$^{-/-}$ had a truncated VL. (H) *Boc*$^{-/-}$. Normal extension of the VL. (I) *Boc*$^{+/-}$*Gas1*$^{-/-}$. Truncated VL. (J) The *Boc*$^{-/-}$*Gas1*$^{-/-}$ compound mutant had an exacerbated VL phenotype with a very short VL and defective incisor tooth germs. Lingual-buccal axes shown in A, same plane in all other images. Mouse numbers analysed: WT (E13.5 *n*>9; E14.5 *n*>3; E15.5 *n*>9; E16.5 *n*>3), *Gas1*$^{-/-}$ *N*=18 (E13.5 *n*=8, E14.5 *n*=4, E15.5 *n*= 3), *Boc*$^{-/-}$ *N*=4 (E13.5 *n*=1; E14.5 *n*=1; E15.5 *n*=1; P0 *n*=1); *Boc*$^{+/-}$*Gas1*$^{-/-}$ *N*=9 (E13.5 *n*=4; E15.5 *n*=3; E18.5 *n*=1; P0 *n*=1); *Boc*$^{-/-}$*Gas1*$^{-/-}$ *N*=3 (E13.5 *n*=1; E15.5 *n*=2). Scale bar: 250 µm.

Gas1 has also been reported to interact with the Hh co-receptor *Boc* in different developmental contexts (Allen et al., 2011). We therefore further explored the function of *Boc* during VL development using mutant mice. Interestingly, analysis of a *Boc* mutant showed a normal VL indistinguishable from WT (Fig. 3C,H) [normal VL observed in *N*=4/4 *Boc*$^{-/-}$ embryos from E13.5 to postnatal day (P) 0]. Loss of a single *Boc* allele in *Gas1*$^{-/-}$ mice did not significantly exacerbate the phenotype compared with *Gas1*$^{-/-}$ mutants (Fig. 3D,I; Fig. 4G) (truncated VL observed in *N*=9/9 *Boc*$^{+/-}$ *Gas1*$^{-/-}$ embryos from E13.5 to P0). In contrast, *Boc/Gas1* double knockouts had exacerbated VL and TB phenotypes, with a severely truncated VL and a developmentally arrested incisor tooth germ (Fig. 3E,J) (severely truncated VL observed in *N*=3/3 *Boc*$^{-/-}$ *Gas1*$^{-/-}$ embryos at E13.5 and E15.5). *Gas1* and *Boc*, therefore, appear to be able to compensate for each other to some extent during VL development.

Downregulation of *Ptch1* and *Gli1* and loss of proliferation in the *Gas1* mutant VL

The identification of a shorter VL in *Gas1*$^{-/-}$ mice suggested that the VL is dependent on Shh signalling for normal development. To confirm this, we assessed expression of *Ptch1* and *Gli1* in these mutants at E13.5, the stage when a clear VL defect is first identifiable in these mice. *Ptch1* was expressed on the labial/buccal side of the VL in WT embryos but, in *Gas1*$^{-/-}$ mice, this expression was lost in the truncated lamina but retained in other regions, including the aboral mesenchyme, underlying the developing whisker follicles (Fig. 4A,D). In the WT, *Gli1*, as viewed by RNAscope, was similarly expressed at significantly higher levels on the buccal side of the VL compared with the lingual side of the VL (Fig. 4B,C,H). Quantification of the RNAscope in the *Gas1*$^{-/-}$ mice revealed that the levels of expression in the buccal epithelium were significantly reduced (Fig. 4E,F,I; Fig. S6) (*N*=3). Given that *Gas1*$^{+/-}$ mice showed a variable truncated VL defect, we assessed changes in *Gli1* in heterozygotes with and without a phenotype at E13.5. In a *Gas1*$^{+/-}$ mouse with no phenotype at this stage, *Gli1* expression appeared as for the WT (Fig. 4M,N). In contrast, *Gas1*$^{+/-}$ mice with a truncated VL still showed *Gli1* expression but had lost the normal buccal-lingual polarity (Fig. 4O). The buccal-lingual difference in Shh response was, therefore, lost in mice with a truncated VL.

To analyse the cause of the truncated phenotype, we investigated the level of proliferation during early development of the VL before the defect in epithelial extension using bromodeoxyuridine (BrdU) to detect cells in the S phase of the cell cycle. At E12.5, the *Gas1*$^{-/-}$ VL and DL were evident as two distinct thickenings, although they appeared to be closer to each other when compared with WT littermates, suggesting part of the phenotype is determined very early in VL development (Fig. 5A-C,G). E-cadherin was used to outline the epithelium and the number of BrdU-positive cells were counted within a defined region, taken from the deepest projection of the DL to the VL (*N*=3) (Fig. 5D-F,H-J, area outlined in D,E,H,I highlights region counted). Proliferation in the epithelium was significantly reduced in the *Gas1*$^{-/-}$ embryos (Fig. 5J,K), with clear reduction of proliferation in the mesenchyme around the forming VL at this stage (Fig. 5D,H).

Loss of *Gas1* activity in the neural crest leads to a truncated VL

Given the strong expression of *Gas1* in both the buccal epithelium and mesenchyme of the VL during development (Fig. 2I,O;

Development (2023) 150, dev201464. doi:10.1242/dev.201464

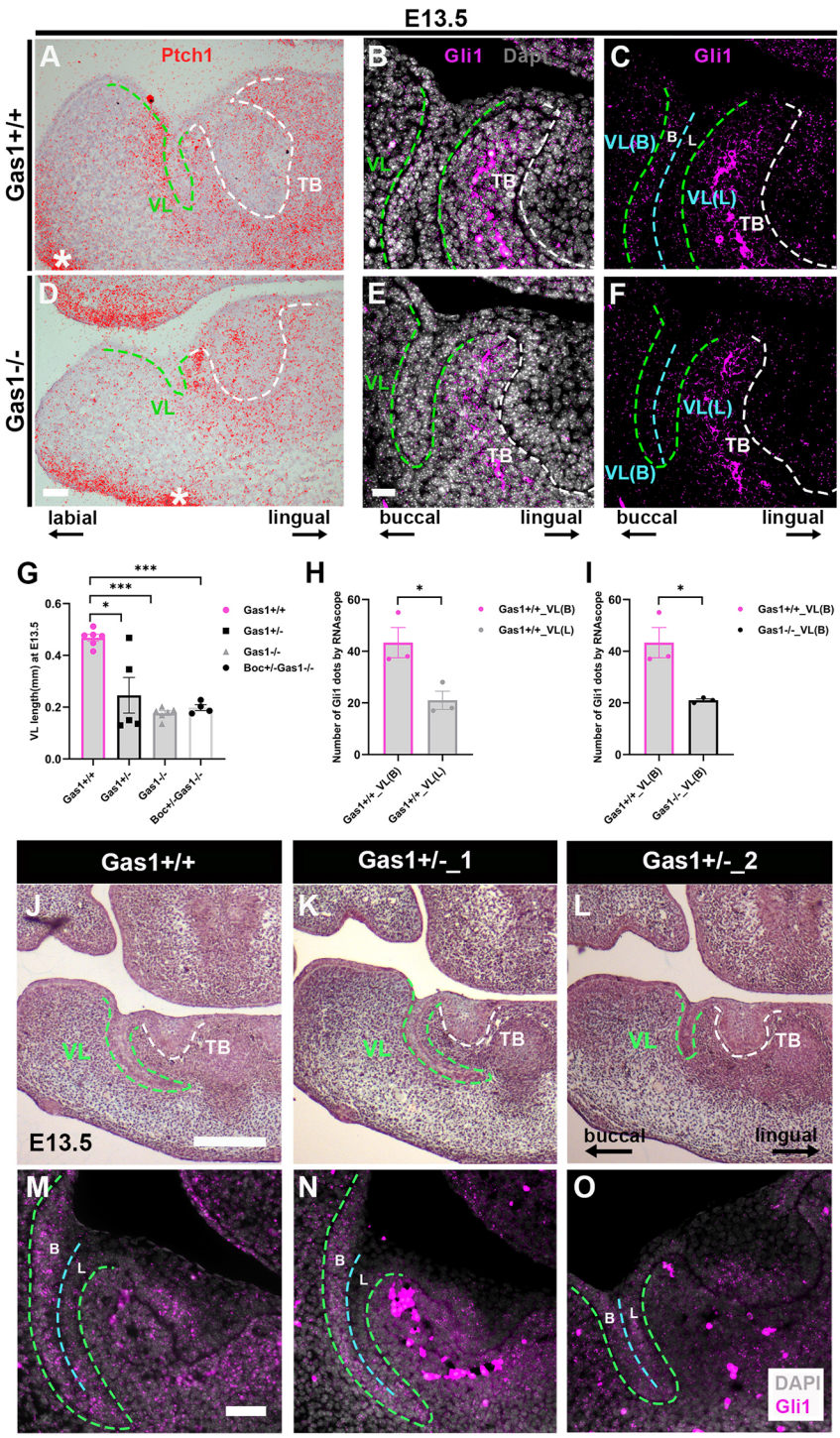

Fig. 4. Altered expression of *Ptch1* and *Gli1* in *Gas1* heterozygote and homozygotes at E13.5. (A,D) Sagittal sections through the lower anterior incisor region showing radioactive *in situ* hybridization of *Ptch1* at E13.5. (A) WT littermate control. (D) $Gas1^{-/-}$. Decreased *Ptch1* expression was observed in the shorter vestibular lamina (VL) in $Gas1^{-/-}$ mice compared with the littermate controls. White asterisks point to the region where the whisker follicles are forming on the aboral side of the jaw, which is *Ptch1*-positive in both. (B,C,E,F) RNAscope in the lower anterior VL in frontal section at E13.5. DAPI (grey), *Gli1* (magenta). (B,C) DAPI and *Gli1* in the littermate controls; (E,F) DAPI and *Gli1* in the $Gas^{-/-}$ mice. The VL was divided by blue dashed lines into two parts: the buccal side [VL(B)], and the lingual side [VL(L)]. (G) Graph showing VL length in WT (N=6), $Gas^{+/-}$ (N=5), $Gas^{-/-}$ (N=6) and $Boc^{+/-}Gas1^{-/-}$ (N=4) at E13.5. The $Gas^{+/-}$ mice present variations in VL length, but show a significantly shortened VL compared with the WT. The $Gas^{-/-}$ mice showed a strikingly consistent shorter VL, with no additional effect with loss of one copy of *Boc*. (H,I) Graphs quantifying *Gli1* expression in the VL. (H) *Gli1* expression on the buccal VL compared with the lingual VL in WT mice. The *Gli1* expression on the buccal side of the VL was significantly higher than the expression on the lingual side of the VL during normal development. N=3, P<0.01. (I) *Gli1* expression on the buccal VL in the WT compared with expression on the buccal VL in $Gas^{-/-}$ mice. Significantly decreased *Gli1* expression was observed on the buccal side of the VL in the $Gas^{-/-}$ mice. (J-L) Trichrome/H&E staining of mouse frontal sections through the lower anterior incisor at E13.5. (J) WT littermate controls. (K) $Gas1^{+/-}$ embryo presenting a normal VL. (L) $Gas1^{+/-}$ embryo presenting a shorter VL. (M-O) RNAscope in the mandible VL in frontal sections. DAPI (grey), *Gli1* (magenta). (M) *Gli1* in the littermate controls. (N,O) *Gli1* in $Gas1^{+/-}$ mice. (N) In the embryo with a WT-shaped VL, the level of *Gli1* was similar to the WT, with higher expression on the buccal side. (O) In the embryo with a truncated VL, the differential expression of *Gli1* on either side of the lamina was lost. Green and white dashed lines delineate the VL and tooth bud (TB), respectively. Lingual-labial axes shown for A,D. Lingual-buccal axes shown for B-F and L, same plane in J,K,M-O. Mouse numbers analysed: WT (E13.5 n>9), $Gas1^{-/-}$ (E13.5 n=8), $Gas1^{+/-}$ (E13.5 n=7), $Boc^{+/-}Gas1^{-/-}$ (E13.5 n=4). *P<0.05, **P<0.01 and ***P<0.001 (two-tailed, unpaired t-test). Error bars represent s.e.m. Scale bars: 50 µm in D (for A,D) and J,M (for J-O); 25 µm in E (for B,C,E,F).

Fig. S5E,F), and reduction of proliferation in both tissues, we wanted to address whether truncation of the VL was caused by loss of *Gas1* in the mesenchyme alone. For this, *Wnt1-Cre;Gas1*$^{fl/fl}$ conditional mutant mice were used. At E16.5, similar to E15.5, the WT VL (labelled by green dashed lines) had extended under the incisors with the ends almost touching each other in the midline in the anterior, and slightly less extended more posteriorly (Fig. 6A,C) (Qiu and Tucker, 2022). Interestingly, *Wnt1-Cre;Gas1*$^{fl/fl}$ mice mimicked the VL phenotype observed in $Gas1^{-/-}$ mice, with a significantly truncated VL that failed to reach past the developing incisors (Fig. 3G compared with Fig. 6B,E) (truncation in N=3/3). *Wnt1-Cre* mice have been shown to have some brain defects but no craniofacial defects (Heuzé et al., 2014), and in keeping with this the VL was normal in all *Wnt1-Cre* controls (N=5/5) (Fig. 6C-E). These findings highlight that loss of *Gas1* in the neural crest-derived mesenchyme alone is sufficient to cause a truncated VL phenotype.

Manipulation of Shh signalling in culture alters VL development

To further manipulate Shh signal levels during early development of the VL, we moved to an *ex vivo* explant culture system, which has previously been used to successfully culture the VL (Qiu and

Development (2023) 150, dev201464. doi:10.1242/dev.201464

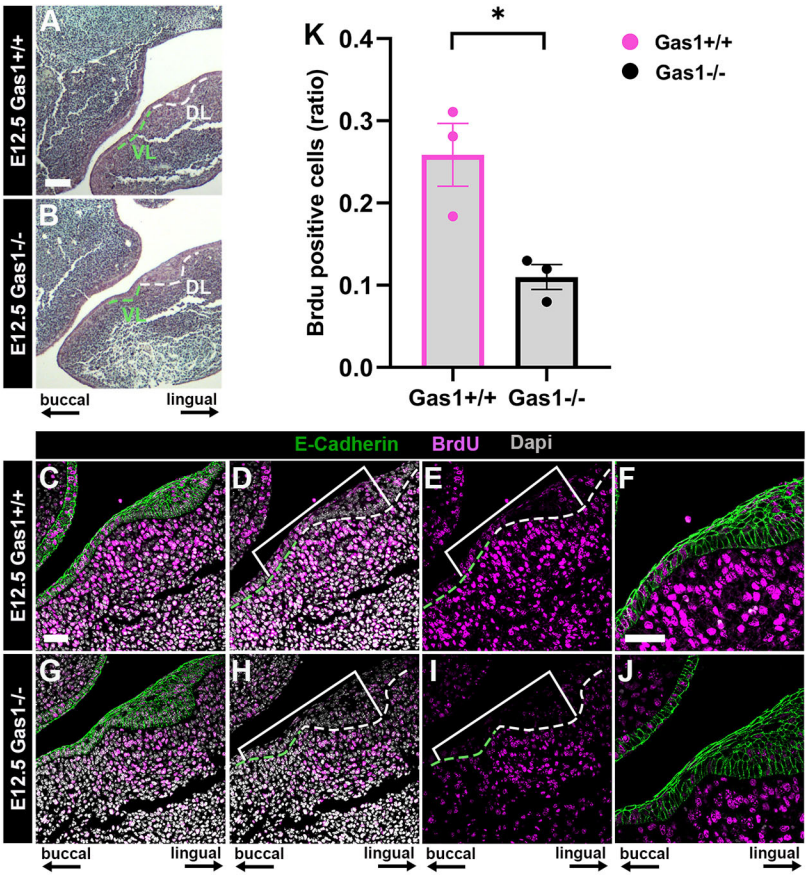

Fig. 5. The truncated VL is associated with reduced proliferation at E12.5. (A,B) Histological (trichrome staining) frontal sections through vestibular lamina (VL) and dental lamina (DL) in the anterior mandible at E12.5. (A) WT littermate control. (B) *Gas1* homozygous mutant. (C-F,G-J) immunofluorescence for E-cadherin (green), BrdU (magenta) and DAPI (grey) in the littermate controls (C-F) and *Gas1*$^{-/-}$ mice (G-J). (C,G) E-cadherin, BrdU and DAPI; (D,H) BrdU and DAPI; (E,I) BrdU; (F,J) Magnification showing a reduced number of BrdU-positive cells in the VL epithelium. (K) Graph comparing the ratio of BrdU-positive cells, where 1=100% of cells are proliferating (N=3, P<0.01, error bars represent s.e.m.). The BrdU-positive cells were significantly decreased in the epithelium in the *Gas1*$^{-/-}$ mice compared with littermate controls. Green and white dashed lines in A,B outline the VL and DL, respectively. The white lines in D, E, H, I define the areas of epithelia selected for counting. Lingual-buccal axes shown for all images. Mouse numbers analysed: WT (E12.5 n>9), *Gas1*$^{-/-}$ (E12.5 n=3). *P<0.05, **P<0.01 and ***P<0.001 (two-tailed, unpaired t-test). Error bars represent s.e.m. Scale bars: 125 µm in A (for A,B); 50 µm in C,F (for C-J).

Tucker, 2022). Here, the mandible harvested at E13.5 was chopped longitudinally into 200 µm thick live slices, and the midline slices containing the VL and incisor tooth germ were selected. Cyclopamine was added at a concentration of 20µM and 50µM to block Shh signalling by interfering with the obligate smoothened receptor (Li et al., 2016). At 20µM whisker follicle development was clearly affected in the slices (Fig. S7), but no obvious VL phenotype was evident (Fig. 7A-D). We therefore increased the concentration to 50µM. Cyclopamine-treated cultures at 50µM continued to grow over the 2 day culture period, with development of a cap stage tooth, but the treated cultures had significantly shorter VLs when compared with slices treated with the carrier solution alone (Fig. 7E-H; Fig. S8) (N=6 control, 6 treated). Confirming loss of Shh signalling, addition of cyclopamine caused an almost complete loss of *Gli1* and *Ptch1* expression (Fig. S10A,C,D,F). To enhance Shh signalling, cultures were treated with SAG (smoothened agonist) at 5µM, which acts to stabilize the key Hh transducer smoothened in the primary cilium. The SAG-treated cultures displayed severe retardation of tooth development and a significant thickening of the forming VL (Fig. 7I-L; Fig. S9) (N=7 control, 7 treated) and was accompanied by an upregulation of *Gli1* in the mesenchyme around the VL and tooth germ and *Ptch1* in the thickened VL (Fig. S10B,E). Targeted loss of Shh signalling at E13.5, therefore, impacted VL development.

DISCUSSION

Distinct lingual-labial/buccal and oral/aboral gene signatures in the VL predate morphological differences

An important aim of this work was to investigate the molecular signature of the VL. The bulk RNA-seq data at E14 provided an interesting set of genes that are likely to play a role in VL development and can be used as markers of the VL in future experiments. Interestingly *Wnt7b* was expressed in the VL, and this gene has been proposed to inhibit Shh expression in non-dental regions (Sarkar et al., 2000). *Meis1/2* were also highlighted in the VL. *Meis1* has been linked to stem cell maintenance and overlaps with *Sox2*-expressing regions, with both *Sox2* and *Meis1* expressed at high levels in the VL (Sanz-Navarro et al., 2019). The VL may, therefore, have some stem cell properties.

One perhaps unexpected result was that many genes exhibited differential expression in the lingual and labial/buccal sides of the VL, suggesting that the epithelium is spatially patterned at this stage, more than 1 week before the VL opens to form the vestibule (Qiu and Tucker, 2022). This differential expression, however, agrees with the observed differences in proliferation rates of the labial/buccal and lingual sides of the VL, which have been proposed to drive the shape of the elongating VL (Qiu and Tucker, 2022). Differences in oral and aboral parts of the VL were also evident, highlighting further compartmentalization of the VL during development. Overall, this is the first molecular analysis of the VL and provides a number of interesting pathways for further exploration.

Shh signalling is essential for correct growth and patterning of the VL

Here, we determined that, although the VL does not express *Shh* after the earliest placodal stages, its development is dependent on Shh signals from the developing tooth. The two laminas are therefore patterning by the same signal. The Shh co-receptors *Gas1*, *Boc* and *Cdon* were shown to have enhanced expression in the

Development (2023) 150, dev201464. doi:10.1242/dev.201464

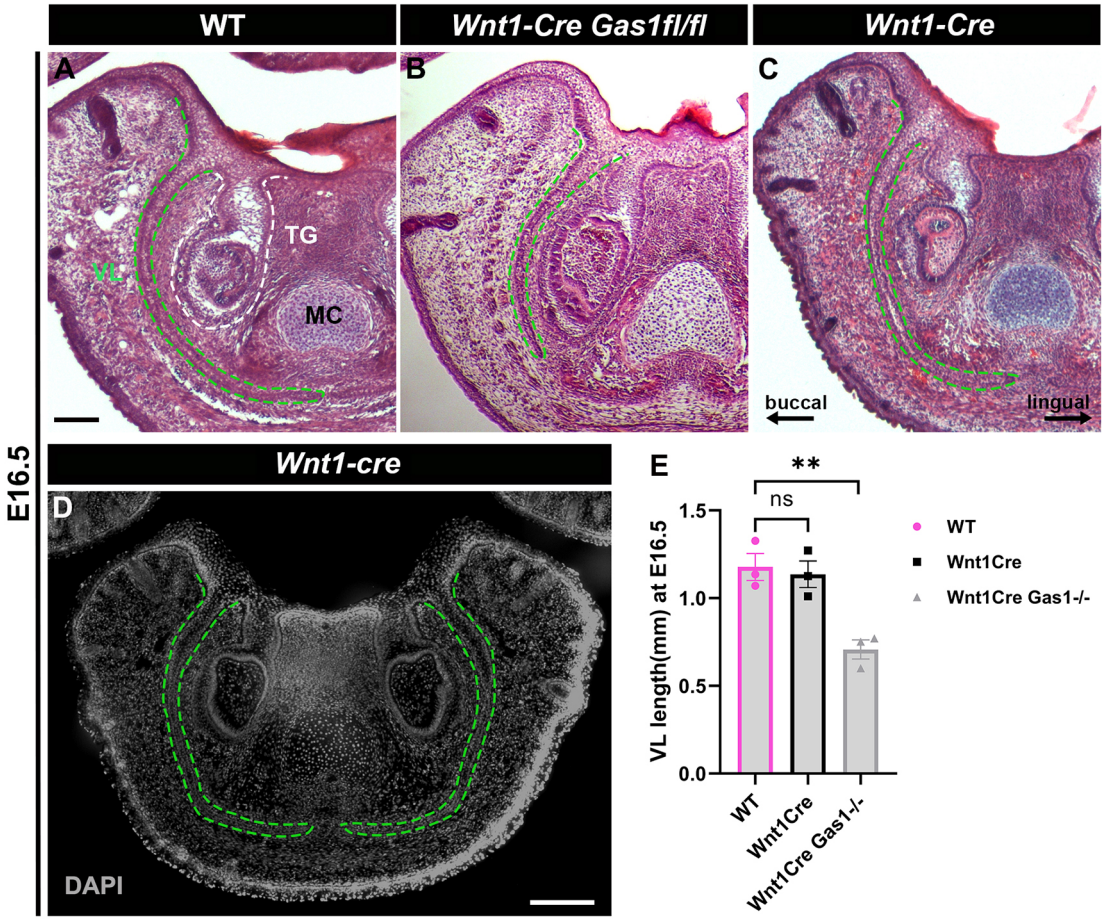

Fig. 6. Lack of *Gas1* in the neural crest in *Wnt1-Cre Gas1*$^{fl/fl}$ embryos mimics the shorter VL phenotype in *Gas1* null mutants. (A-C) H&E staining of the anterior lower jaw in frontal sections at E16.5 showing WT (A), *Wnt1-Cre Gas1*$^{fl/fl}$ (B) and *Wnt1-Cre* (C) mice. A shorter vestibular lamina (VL) was observed in the *Wnt1-Cre Gas1*$^{fl/fl}$ mice compared with the WT and *Wnt1-cre* positive control, mimicking the VL phenotype in the *Gas1*$^{-/-}$ mice (Fig. 3B,G). (D) A normal VL was observed in *Wnt1-Cre* mice; DAPI nuclear stain (grey). (E) Graph showing VL length in the WT (*N*=3, s.e.m.), *Wnt1-Cre* (*N*=3, s.e.m.), and *Wnt1-Cre Gas1*$^{fl/fl}$ (*N*=3, s.e.m.) mice at E16.5. The VL in the *Wnt1-Cre Gas1*$^{fl/fl}$ mice was significantly shorter compared to the WT. Green dashed lines label the VL in A-D. TG, tooth germ; MC, Meckel's cartilage. Lingual-buccal axes shown in C, same axes for all images. **P*<0.05, ***P*<0.01 and ****P*<0.001 (two-tailed, unpaired *t*-test). ns, not significant. Error bars represent s.e.m. Scale bars: 125 µm in A (for A-C); 200 µm in D.

forming VL, and loss of *Gas1* in mouse mutants resulted in truncation of the forming VL. Failure in extension of the VL was driven by a reduction/misexpression of readouts of Hh signalling and a reduction in proliferation. Interestingly, *Gas1* heterozygous mice showed a variable defect in the VL, correlating to changes in *Gli1* expression. *Gas1* heterozygous mice are viable and feed as normal, suggesting that earlier VL defects may be able to correct themselves during later development. This may be linked with developmental stalling, whereby mutant mice display initial defects and a slowing down of development but are able to recover with later accelerated development (Miletich et al., 2011). In both homozygotes and heterozygous *Gas1* mutants the truncated VL was linked to a loss of the differential expression of *Gli1* in the epithelium, suggesting that the lingual-buccal/labial differences are key drivers of vestibular lamina outgrowth.

Gas1 in the VL mesenchyme extends the range of the Shh signal

Gas1 mutants have previously been shown to have tooth defects, which include fusion of the first and second molars, formation of supernumerary teeth in the diastema and cusp defects (Seppala et al., 2022). Loss of one copy of *Boc* in *Gas1* mutants did not exacerbate the phenotype but loss of two copies in the compound mutants resulted in very severe VL defects. *Boc* and *Gas1* have been shown to form distinct complexes with *Ptch1* (Izzi et al., 2011). *Boc*$^{-/-}$ are viable, with subtle changes to the cerebellum and a background-dependent mild widening of the facial region (Izzi et al., 2011; Echevarriá-Andino and Allen, 2020). Interestingly, although in many tissues loss of both *Boc* and *Gas1* leads to a worsening of the single mutant phenotype (Seppala et al., 2014), with regards to the width of the face, *Boc* and *Gas1* double mutants had a less severe craniofacial phenotype, suggesting context-dependent effects of these two co-receptors (Echevarriá-Andino and Allen, 2020). Similarly, *Gas1* can restrain, rather than enhance, Hh signalling in the mouse diastema and in presomitic mesoderm explants (Lee et al., 2001a; Cobourne et al., 2004). In the VL, however, *Boc* and *Gas1* appear to act by facilitating Shh signalling in tissue at a distance from the Shh source, with a significant downregulation of *Gli1* in the VL of *Gas1* mutants, particularly on the buccal/labial side. A proposed model of Hh signalling in the VL is shown in Fig. 8, highlighting the known role of the primary cilium. This agrees with findings in the heart, neural tube and limb (Martinelli and Fan, 2007). In these tissues, Shh has been shown to downregulate *Gas1* to constrain its own activity, which may explain

Development (2023) 150, dev201464. doi:10.1242/dev.201464

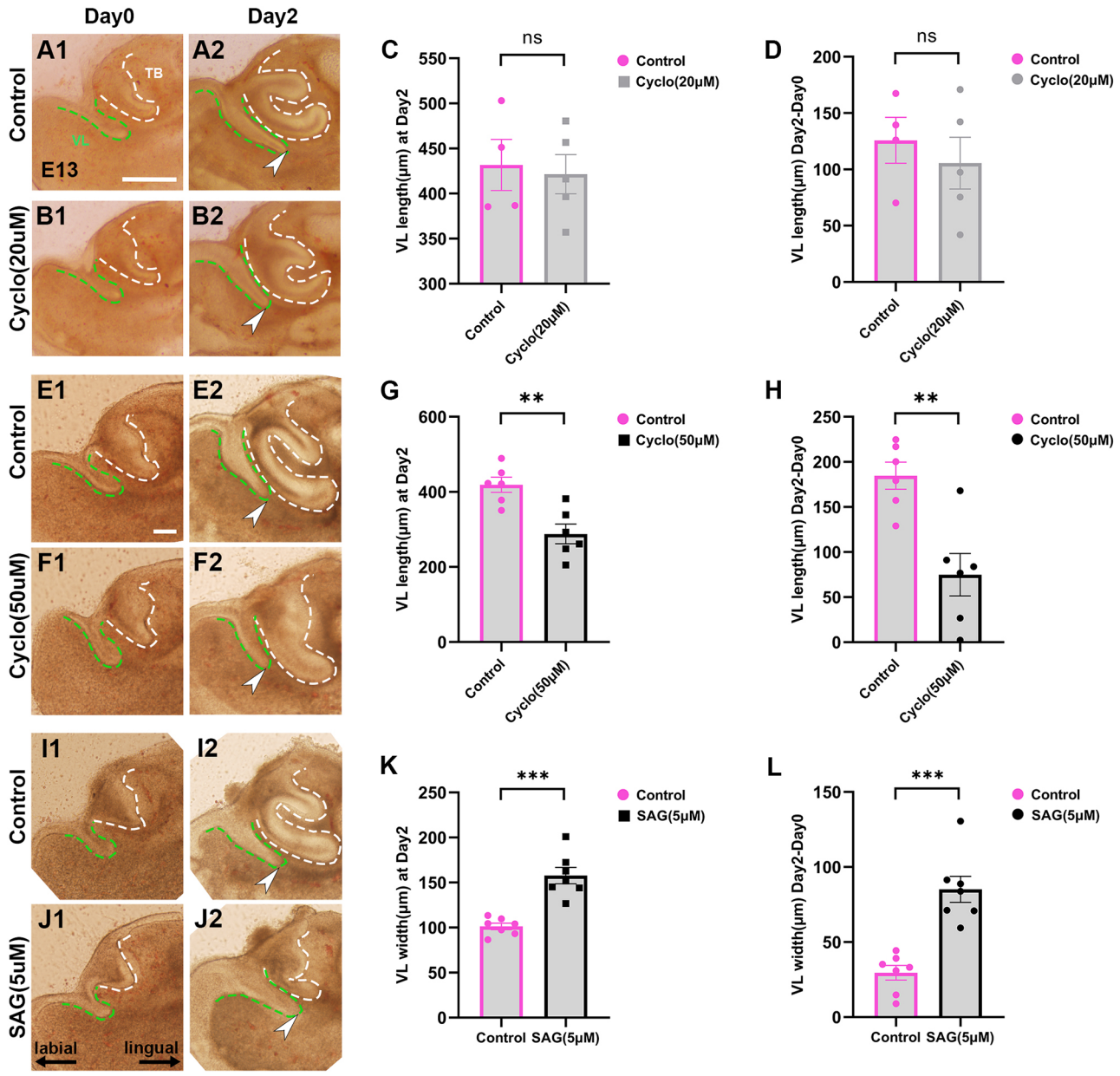

Fig. 7. Manipulation of Shh signalling in explant culture led to changes in VL length and width. (A-J) Sagittal explant slices through the anterior mandible at E13.5. (A1,B1,E1,F1,I1,J1) Day 0. Prominent vestibular lamina (VL) and tooth bud (TB) were observed at E13.5. (A2,B2,E2,F2,I2,J2) Day 2. The VL protruded into the mesenchyme following the curve of the forming tooth germ after 48 h in culture. (A1,2) Control carrier only group for cyclopamine-treated cultures (20 µM). (B1,2) Cyclopamine-treated cultures (20 µM). (E1,2) Control carrier only group for cyclopamine-treated cultures (50 µM). (F1,2) Cyclopamine-treated cultures (50 µM). (I1,2) Control group for SAG-treated cultures (5 µM). (J1,2) SAG-treated group. (B2,C) The VL was not significantly shorter in the cyclopamine-treated cultures at a concentration of 20 µM (N=5) compared with the controls (N=4) after 2 days in culture. (D) To account for any variation at the start of culture we also compared the increase in length during culture by analysing the length at day 2 minus the length at day 0. This also showed no significant difference. (F2,G,H) When treated with 50 µM cyclopamine, the VL was significantly shorter in the cyclopamine-treated cultures (N=6 for both) after 2 days in culture using both measures. (J2,K,L) The VL was significantly thicker in the SAG-treated (5 µM) cultures (N=7 for both) after 2 days in culture (K). In addition, we compared the VL width difference on day 2 minus day 0 and showed a statistical significance (L). Green dashed lines label the VL and white dashed lines outlined the TB. White arrowheads indicate tip of VL after culture. Lingual-labial axes shown in J1, same orientation for all images. *P<0.05, **P<0.01 and ***P<0.001 (two-tailed, unpaired t-test). Error bars represent s.e.m. All experiments were repeated more than six times for SAG and 50 µM cyclopamine, and four times for 20 µM cyclopamine, and differences were compared within a litter. Scale bars: 300 µm in A1 (for A1,A2,B1,B2); 100 µm in E1 (for E1,E2,F1,F2,I1,I2,J1,J2).

the heightened expression of *Gas1* in the VL compared with the tooth in WT embryos.

Gas1 was expressed in both the buccal/labial epithelium of the VL and the surrounding mesenchyme. Perhaps unexpectedly, loss of *Gas1* in the neural crest-derived mesenchyme alone led to truncation of the VL. Expression in the epithelium is therefore not sufficient for VL extension. Tooth number has similarly been found to be dependent on *Gas1* expression in the mesenchyme, with supernumerary teeth developing in the diastema of *Wnt1-Cre; Gas1*$^{fl/fl}$ mice (Seppala et al., 2022).

Development (2023) 150, dev201464. doi:10.1242/dev.201464

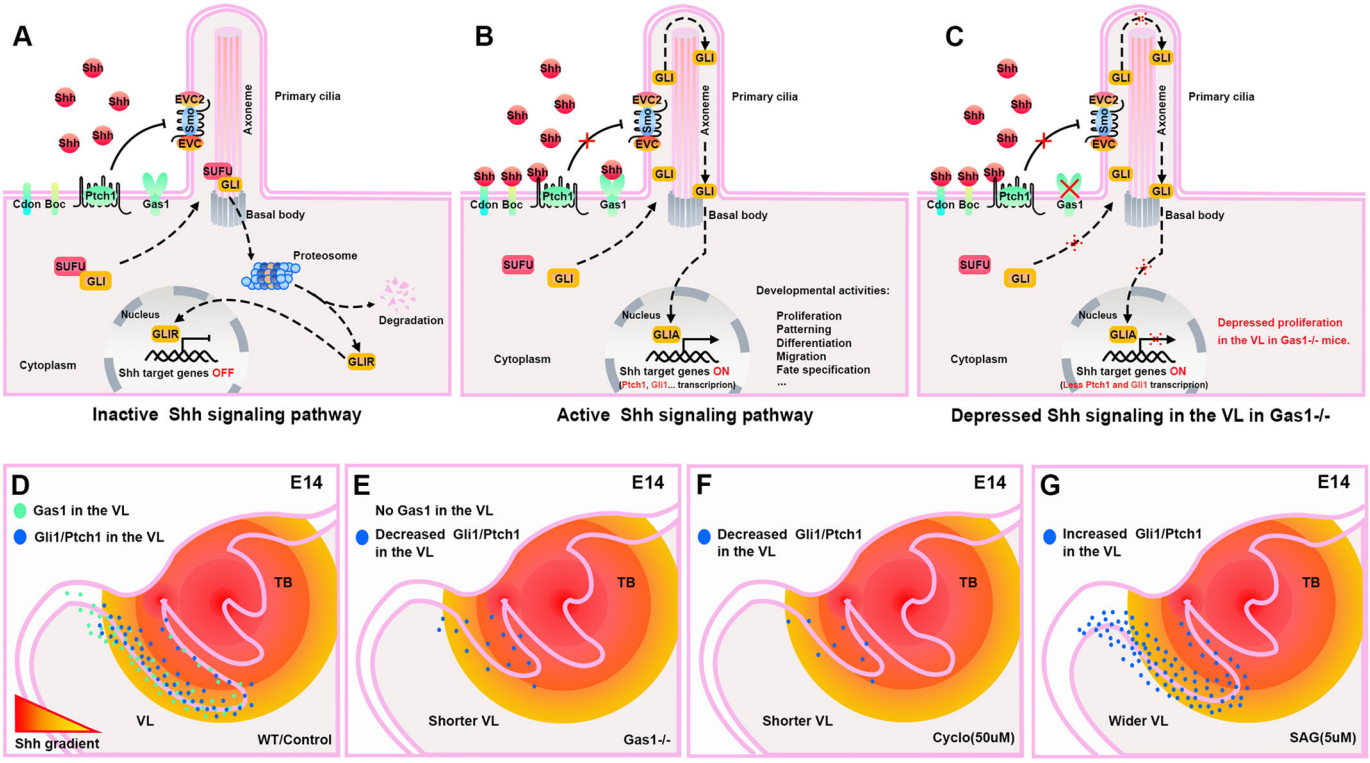

Fig. 8. Schematic of Shh signalling in the VL. (A,B) Review of vertebrate Shh signalling at the cell membrane (Caparrós-Martín et al., 2013; Seppala et al., 2017). (A) Inactive Shh signalling pathway (Off). In the absence of Shh signal, the cell surface receptor Ptch1 accumulates at the primary ciliary membrane and inhibits Smo. GLI proteins are sequestered by SuFu, and proteolytically processed into truncated repressor forms, thus repressing the pathway transcription. (B) Active Shh signalling pathway (On). With the arrival of secreted Shh, the signalling pathway is activated when Shh binds to Ptch1 and releases the inhibition to Smo. This is facilitated by the co-receptors Cdon, Boc and Gas1. The activated Smo enters into the primary cilia and interacts with the EVC/EVC2 complex to trigger the downstream GLI family transcriptional activities. Gli1 translocates into the nucleus to promote the target gene expression. (C) Depressed Shh signalling in *Gas1* homozygous mutants. In the *Gas1*$^{-/-}$ mutant VL, it is proposed that low levels of Shh cannot release the inhibition of Smo owing to loss of a key co-receptor, leading to reduced activation of Gli1 in the VL. (D-G) Schematics of the activity of Shh in the vestibular lamina (VL). (D) In the WT, Shh is produced in the tooth germ and diffuses in a gradient away from the source. High levels of *Gas1* at a distance from the Shh source allow upregulation of *Gli1* and *Ptch1* in the VL. Expression of Hh downstream pathway genes is essential for proliferation and extension of the VL. (E) In *Gas1* mutants, the normal Shh signal at the VL is too weak to elicit activation of *Gli1* and *Ptch1* and the VL fails to grow. (F) In the presence of the smoothened inhibitor cyclopamine, again *Gli1* and *Ptch1* are not activated in the VL and it fails to grow. (G) On stimulation of smoothened by SAG, cells further away from the Shh source can respond and the pathway is upregulated, leading to increase in the width of the VL.

Requirement for Hedgehog signalling in the VL explains the frenula defects observed in EvC patients

Vestibule defects are associated with EvC syndrome, where the gums adhere to the upper lip and cheek with multiple associated frenula (Sasalawad et al., 2013). Interestingly, *Evc* also has a role in the Shh pathway, interacting with smoothened in the primary cilium (Fig. 8). *Evc* regulates Hh signalling by promoting Sufu/Gli3 dissociation and Gli3 ciliary traffic (Caparrós-Martín et al., 2013). A *lacZ Evc* reporter has previously shown expression of *Evc* around the teeth and VL at E15.5 (Ruiz-Perez et al., 2007). The VL has not been studied in *Evc* mutant mice, but a similar truncated VL might be predicted based on a reduction in the Hh pathway and the phenotype from the *Gas1* mutants. VL defects would also be predicted to occur in other ciliopathies and, in keeping with this, frenula defects have been noted in oral-facial-digital (OFD) syndromes (Bruel et al., 2018) and in Joubert syndrome (Penon-Portmann et al., 2022). OFD syndromes can be caused by defects in the ciliary basal body, ciliogenesis or post-ciliary microtubule functions, with at least 20 genes identified in patients (Bruel et al., 2018). It would, therefore, be interesting to study the VL in mouse models where primary cilia function is disrupted. In addition, changes in the vestibule, with defects and accessory frenula, may represent an important additional clinical character for defining ciliopathies in patients.

Variation in Hedgehog signalling may explain species-specific difference in the VL

Our culture experiments allowed the development of the VL and tooth germ to be followed and the Hh pathway to be manipulated at specific time points. Addition of cyclopamine or SAG to target smoothened led to striking defects in the VL. Agreeing with the results from the *Gas1* mutants, addition of cyclopamine caused a shorter VL that failed to extend into the surrounding mesenchyme, strengthening the results that *Gas1* promotes Hh signalling in the VL. Addition of SAG led to a broadening of the VL, which we hypothesize was caused by an extension of the tissue that was able to respond to Shh produced by the neighbouring tooth germ (Fig. 8). The width of the VL varies considerably across mammals, therefore, the wider VL of humans may be driven by enhanced Hh signalling in this tissue compared with mammals such as the mouse, where the VL is very thin.

The results highlight that the tooth germ, through Hh signalling, plays a key role in development of the VL. These two neighbouring laminas, therefore, not only share a common origin in some parts of the jaw but are later patterned together. Defects in the tooth are, therefore, likely to result in defects in the VL. The VL is a fairly unstudied structure, therefore, many published mouse mutants with dental defects may have unreported defects in the VL. From an

Development (2023) 150, dev201464. doi:10.1242/dev.201464

evolutionary perspective, changes to the dentition might not change in isolation but involve secondary effects on the vestibule, linking the evolutionary history of these two structures.

MATERIALS AND METHODS

Mouse strains

Gas1 mutant mice were generated as previously described (Lee et al., 2001b; Seppala et al., 2022). *Gas*$^{+/-}$ (Lee et al., 2001b) and *Boc*$^{+/-}$ (Okada et al., 2006), *Wnt1-Cre*$^{+/-}$ (Danielian et al., 1998) and *Gas1*$^{fl/+}$ (Jin et al., 2015) were crossed to generate compound and conditional mutant mice, respectively. The mice analysed in this research are listed below: WT (E12.5 n>9; E13.5 n>9; E14.5 n>3; E15.5 n>9; E16.5 n>3), *Gas1*$^{-/-}$ N=18 (E12.5 n=3; E13.5 n=8, E14.5 n=4, E15.5 n= 3), *Gas1*$^{+/-}$ N=13 (E12.5 n=3; E13.5 n=7; E14.5 n=3), *Boc*$^{-/-}$ N=4 (E13.5 n=1; E14.5 n=1; E15.5 n=1; P0 n=1); *Boc*$^{+/-}$ *Gas1*$^{-/-}$ N=9 (E13.5 n=4; E15.5 n=3; E18.5 n=1; P0 n=1); *Boc*$^{-/-}$ *Gas1*$^{-/-}$ N=3 (E13.5 n=1; E15.5 n=2); *Wnt1-Cre*;*Gas1*$^{fl/fl}$ N=3 (E16.5), *Wnt1-Cre* N=5 (E16.5). Mutant mice and littermate controls were on a mixed 129sv/C57Bl6 background (Seppala et al., 2022). CD1 mice for transcriptomics, explant culture and *in situ* hybridization were obtained at the Institute of Animal Physiology and Genetics, Czech Academy of Sciences, and King's College London. E0.5 was considered as the day when the plug was detected. All animal procedures were carried out under the guidelines of the Institute of Animal Physiology and Genetics, and King's College London, with Home Office approved Schedule 1 culling methods and conform to ARRIVE guidelines. For proliferation assays, BrdU (30 mg/kg) was injected into the pregnant mouse 2 h before culling.

RNA isolation and RNA-seq library construction and sequencing

VL and neighbouring incisor tooth germs were isolated from the same slices at E14. The dissected VL and tooth germs from a single litter (9-15 embryos) were pooled to obtain enough RNA for sequencing. In total, tissue from 11 litters was isolated at this stage. RNA extraction was performed using the RNeasy Plus Mini Kit (Qiagen, 74136) and pooled samples from five litters with the highest quality scores were used for analysis. These are referred to here as TB1-5 and VL1-5. Sequencing libraries were prepared from total RNA using the Smarter Stranded Total RNA-seq Kit v2 Pico Input Mammalian (Takara), followed by size distribution analysis in the Agilent 2100 Bioanalyzer using a High Sensitivity DNA Kit (Agilent, 5067-4626). Libraries were sequenced using the Illumina NextSeq 500 instrument. Samples were sequenced by the Genomics service at the Institute of Molecular Genetics. Tuxedo protocol was performed for Genome-guided assembly.

Downstream analysis of RNA-seq

The RNA-seq datasets were visualized using R (v4.0.2). Duplicated genes and genes with zero read counts were removed. The counts per gene were normalized to CPM transformed with log2 using an offset of 1. Expression plots such as box plot, violin plot and density plot were generated using package ggplot2 (v3.3.5). Two-tailed, unpaired *t*-test was performed for statistical significance of comparisons in gene expression visualized in box plots. PCA was performed using package pca3d (v0.10.2). Correlation matrix was visualized using package corrplot (v0.90). For differential expression analysis, package limma (v3.46.0) was used to identify the DEGs in TB and VL groups (N=5 in each group). The cut-off criteria for DEGs were set up with the abs log2FC>1.5 and P-value<0.05. Heatmaps and volcano plots were depicted to visualize the results using the packages pheatmap (v1.0.12), ggplot2 (v3.3.5), dplyr (v1.0.7) and ggrepel (v0.9.1). To prioritize genes of interest, two groups of criteria were established in volcano plots with the abs log2FC_1>1, P-value_1<0.05, and abs log2FC_2>2, P-value_2<0.01. The genes were filtered with settings of the abs log2FC>2 and P-value<0.001 in Heatmap showing ranked genes with highest differential expression.

Tissue processing and histological staining

Embryonic heads were fixed in 4% paraformaldehyde (PFA) overnight at 4°C followed by gradient dehydration in ethanol, xylene clearance, wax immersion and paraffin embedding. Samples were then sectioned at 5-8 µm using a microtome (Leica RM2245) and mounted on the charged slides in series sections. For histological analysis, the slides were stained with Haematoxylin and Eosin (H&E) staining, or trichrome staining (Sirrus Red, Haematoxylin and Alcian Blue) using standard protocols. The Nikon Eclipse 80i light microscope was used to photograph the stained slides.

Immunofluorescence staining

Immunostaining was performed using standard protocols as previously described (Qiu et al., 2020; Qiu and Tucker, 2022). The primary antibodies used on sections were: mouse anti-E-cadherin (Abcam, ab76055, 1/400) and rat anti-BrdU (Abcam, ab6326, 1/500). Secondary antibodies were then used to incubate the sections for 1 h at room temperature (RT) at a dilution of 1/500 in the dark: Alexa Fluor donkey anti-mouse 488 (Invitrogen, A21202) and Alexa Fluor donkey anti-rat 647 (Invitrogen, A21247). Slides were mounted with Fluoroshield containing DAPI (Sigma-Aldrich, SLBV4269) and visualized using a Leica TCS SP5 confocal microscope. For BrdU immunofluorescence staining, the mice were injected with BrdU labelling reagent (30 mg/kg, Life Technologies, 000103) 2 h before collection. For E-cadherin immunofluorescence on slices, rabbit anti-E-cadherin (Abcam, ab15148, 1:100) with secondary Fluor goat anti-rabbit 488 (Invitrogen, A-11008, 1:500). Control groups were set up to confirm immunofluorescence staining. Each antibody analysis was carried out at least three times independently.

Radioactive *in situ* hybridization

Radioactive section *in situ* hybridization was performed as previously described (Wilkinson, 1992; Seppala et al., 2014). RNA probes were synthesized using ^{35}S-UTP, and signals were recognized using silver emulsion, which presents positive signals as white grains when viewed under dark-field. Bright-field and dark-field images were photographed using a Nikon Eclipse 80i light microscope. The images were then merged in Photoshop (Adobe 2020), with the colour in dark-field artificially changed to red. The following restriction and polymerase enzymes were used for plasmid DNA linearization and mRNA probe synthesis; EcorI and T7 for *Shh*, BamHI and T3 for *Ptch1*, EcorI and T7 for *Gas1*, XhoI and T7 for *Cdon*, SalI and T7 for *Boc*. We would like to thank Andrew McMahon (Harvard University, USA) for the *Shh* plasmid, Matthew Scott (Stanford University, USA) for the *Ptch1* plasmid, Chen-Ming Fan (Carnegie Institution of Washington, USA) for the *Gas1* plasmid and Robert Krauss (Icahn School of Medicine at Mount Sinai, USA) for the *Cdon* and *Boc* plasmids.

RNAscope assay

Paraffin-embedded embryonic head sections (5 µm) were processed as described above for multiplex fluorescent *in situ* hybridization. Commercially available Multiplex Fluorescent Reagent Kit v2 (323100, Advanced Cell Diagnostics) and RNAscope probes (1:50; Mm-Gli1, 311001; Mm-Meis1, 436361; Mm-Meis2, 436371; Mm-Cd44, 476201; Mm-Nr4a2, 423351; Mm-Wnt7b, 401131; Mm-Otx1, 536041; Mm-Dlx5, 478151; Mm-Runx2, 414021; Mm-Rspo1-O1, 479591; Mm-Scube1, 488131; Mm-Shh, 314361; Mm-Gas1, 547201; Mm-Ptch1, 402811; Advanced Cell Diagnostics) were used for transcript detection according to the manufacturer's protocol. The hybridized probes were visualized using the fluorescein (NEL741001KT, Perkin Elmer) and TSA-Plus Cyanine 3 (NEL744001KT, Perkin-Elmer) system, according to the manufacturer's protocol. All incubation steps were completed using the ACD HybEZ II Hybridization System (321721) at 40°C. In brief, the slides were deparaffinized in xylene, applied in RNAscope Hydrogen Peroxide (322335) at RT for 10 min and submerged in RNAscope Target Retrieval (322001) at 99°C for 30 min. A hydrophobic barrier was then created to circle the interested areas using the ImmEdge Hydrophobic Barrier Pen (310018). Slides were then incubated with RNAscope Protease III (322340) for 15 min followed by the hybridization, amplification and detection steps according to the protocol. Slides were mounted with Fluoroshield with DAPI (Sigma-Aldrich, SLBV4269) and stored at 4°C in the dark.

Statistics and reproducibility

Quantification of *Gli1* expression levels from RNAscope is outlined in Fig. S6. Morphometrics of structures were performed using Fiji/ImageJ. The length of the VL was assessed by drawing a line parallel to the curved VL from the top to the end using the line tool in Fiji. The width of the VL was measured by drawing a line parallel to the oral epithelium from the junction of VL and DL to the edge of the buccal VL. Results were plotted in GraphPad Prism software (V.8.0.2). Statistical significance was analyzed by IBM SPSS Statistics software (V.25.0) using two-tailed, unpaired *t*-tests. The *P*-values were considered statistically significant if the *P*-value<0.05, with **P*<0.05, ***P*<0.01 and ****P*<0.001. Error bars represent s.e.m.

Explant culture

Slice culture for the tooth germ was carried out as previously described (Alfaqeeh and Tucker, 2013). In brief, embryonic lower jaws were isolated at E13.5, when a very clear VL/DL bud can be observed. The mandibles were then chopped sagittally at 200 µm using a McIlwain Tissue Chopper, and slices in the incisor region were selected and cultured on permeable filters (pore size 0.4 µm, BD Falcon cell culture inserts) held by a steel mesh in Advanced Dulbecco's Modified Eagle Medium F12 (DMEM F12) (Invitrogen) with 1% penicillin-streptomycin (Sigma-Aldrich, Merck) and 1% Glutamax (Invitrogen). To investigate the role of Shh during VL development, slices were cultured with Shh signalling inhibitor cyclopamine (Sigma-Aldrich) at 20 µM or 50 µM (10 mg/ml stock in ethanol), or SAG (smoothened agonist) (Sigma-Aldrich) at 5 µM (stock dissolved in H_20). The explants were cultured at 5% CO_2 and 37°C for 2 days before harvest. Littermate control groups were set up to compare with the experimental groups and cultured under the same conditions but with carrier alone. Litter age can vary depending on mating time, so cultures were only compared within litters. Slices were photographed at day 0 and day 2 using a Leica dissecting microscope to record the morphology. All experiments were repeated more than six times for SAG and 50 µM cyclopamine, and four times for 20 µM cyclopamine.

Acknowledgements

We thank Chen-Ming Fan (Carnegie Institution of Washington) for generously providing us with the *Gas1* mutant line and compound mutant embryos.

Competing interests

The authors declare no competing or financial interests.

Author contributions

Conceptualization: M.H., M.B., A.S.T.; Methodology: T.Q., B.H., M.S., M.T.C., Z.C., M.H., A.S.T.; Formal analysis: T.Q., B.H., M.H., M.B.; Investigation: T.Q., B.H., M.S., M.H.; Resources: M.S., M.T.C., Z.C., A.S.T.; Data curation: M.S., M.H., M.B.; Writing - original draft: T.Q.; Writing - review & editing: M.T.C., Z.C., M.H., M.B., A.S.T.; Supervision: Z.C., M.B., A.S.T.; Project administration: A.S.T.; Funding acquisition: T.Q., Z.C., M.B., A.S.T.

Funding

This work was funded by a grant from the Grantová Agentura České Republiky (21-04178S) awarded to A.S.T. and M.B. Transcriptomics was supported by a previous grant (18-04859S). Additional funds were provided by the National Natural Science Foundation of China (NSFC82230029) and an Open Research Fund Program grant (Hubei-MOST KLOS & KLOBM 2020-04) from Wuhan University to T.Q., A.S.T. and Z.C. T.Q. was funded by the China Scholarship Council as part of a PhD studentship at King's College London. M.T.C. and M.S. are funded by a research grant from the European Orthodontic Society.

Data availability

The transcriptomic dataset used in this study is publicly available at Facebase (https://www.facebase.org/) (Tucker et al., 2023).

Peer review history

The peer review history is available online at https://journals.biologists.com/dev/lookup/doi/10.1242/dev.201464.reviewer-comments.pdf.

References

Alfaqeeh, S. A. and Tucker, A. S. (2013). The slice culture method for following development of tooth germs in explant culture. *J. Vis. Exp.* e50824.

Allen, B. L., Song, J. Y., Izzi, L., Althaus, I. W., Kang, J. S., Charron, F., Krauss, R. S. and Mcmahon, A. P. (2011). Overlapping roles and collective requirement for the coreceptors GAS1, CDO, and BOC in SHH pathway function. *Dev. Cell* **20**, 775-787. doi:10.1016/j.devcel.2011.04.018

Bolk, L. (1921). Odontological Essays. *J. Anat.* **55**, 219-234.

Bruel, A.-L., Levy, J., Elenga, N., Defo, A., Favre, A., Lucron, H., Capri, Y., Perrin, L., Passemard, S., Vial, Y. et al. (2018). INTU-related oral-facial-digital syndrome type VI: A confirmatory report. *Clin. Genet.* **93**, 1205-1209. doi:10.1111/cge.13238

Buchtová, M., Handrigan, G. R., Tucker, A. S., Lozanoff, S., Town, L., Fu, K., Diewert, V. M., Wicking, C. and Richman, J. M. (2008). Initiation and patterning of the snake dentition are dependent on Sonic Hedgehog signaling. *Dev. Biol.* **319**, 132-145. doi:10.1016/j.ydbio.2008.03.004

Caparrós-Martín, J. A., Valencia, M., Reytor, E., Pacheco, M., Fernandez, M., Perez-Aytes, A., Gean, E., Lapunzina, P., Peters, H., Goodship, J. A. et al. (2013). The ciliary EVC/EVC2 complex interacts with smo and controls hedgehog pathway activity in chondrocytes by regulating Sufu/Gli3 dissociation and Gli3 trafficking in primary cilia. *Hum. Mol. Genet.* **22**, 124-139. doi:10.1093/hmg/dds409

Cobourne, M. T., Miletich, I. and Sharpe, P. T. (2004). Restriction of sonic hedgehog signalling during early tooth development. *Development* **131**, 2875-2885. doi:10.1242/dev.01163

Danielian, P. S., Muccino, D., Rowitch, D. H., Michael, S. K. and Mcmahon, A. P. (1998). Modification of gene activity in mouse embryos in utero by a tamoxifen-inducible form of cre recombinase. *Curr. Biol.* **8**, 1323-1326. doi:10.1016/S0960-9822(07)00562-3

Echevarrıá-Andino, M. L. and Allen, B. L. (2020). The hedgehog co-receptor BOC differentially regulates SHH signaling during craniofacial development. *Development (Camb.)* **147**, dev189076. doi:10.1242/dev.189076

Heuzé, Y., Singh, N., Basilico, C., Jabs, E. W., Holmes, G. and Richtsmeier, J. T. (2014). Morphological comparison of the craniofacial pehenotypes of mouse models expressing th Apert FGFR2 S252W muation in neural crest or mesoderm derived tissues. *Bone* **63**, 1001-1109. doi:10.1016/j.bone.2014.03.003

Hovorakova, M., Lesot, H., Peterka, M. and Peterkova, R. (2005). The developmental relationship between the deciduous dentition and the oral vestibule in human embryos. *Anat. Embryol.* **209**, 303-313. doi:10.1007/s00429-004-0441-y

Hovorakova, M., Lesot, H., Vonesch, J.-L., Peterka, M. and Peterkova, R. (2007). Early development of the lower deciduous dentition and oral vestibule in human embryos. *Eur. J. Oral Sci.* **115**, 280-287. doi:10.1111/j.1600-0722.2007.00464.x

Hovorakova, M., Lochovska, K., Zahradnicek, O., Domonkosova Tibenska, K., Dornhoferova, M., Horakova-Smrckova, L. and Bodorikova, S. (2016). One odontogenic cell-population contributes to the development of the mouse incisors and of the oral vestibule. *PLoS ONE* **11**, e0162523. doi:10.1371/journal.pone.0162523

Hovorakova, M., Zahradnicek, O., Bartos, M., Hurnik, P., Stransky, J., Stembirek, J. and Tucker, A. S. (2020). Reawakening of ancestral dental potential as a mechanism to explain dental pathologies. *Integr. Comp. Biol.* **60**, 619-629. doi:10.1093/icb/icaa053

Izzi, L., Lévesque, M., Morin, S., Laniel, D., Wilkes, B. C., Mille, F., Krauss, R. S., Mcmahon, A. P., Allen, B. L. and Charron, F. (2011). Boc and Gas1 each form distinct Shh receptor complexes with Ptch1 and are required for Shh-mediated cell proliferation. *Dev. Cell* **20**, 788-801. doi:10.1016/j.devcel.2011.04.017

Jin, S., Martinelli, D. C., Zheng, X., Tessier-Lavigne, M. and Fan, C. M. (2015). Gas1 is a receptor for sonic hedgehog to repel enteric axons. *Proc. Natl. Acad. Sci. USA* **112**, E73-E80. doi:10.1073/pnas.1418629112

Kantaputra, P. N., Wangtiraumnuay, N., Ngamphiw, C., Olsen, B., Intachai, W., Tucker, A. S. and Tongsima, S. (2022). Cryptophthalmos, dental anomalies, oral vestibule defect, and a novel FREM2 mutation. *J. Hum. Genet.* **67**, 115-118. doi:10.1038/s10038-021-00972-4

Kawasaki, M., Porntaveetus, T., Kawasaki, K., Oommen, S., Otsuka-Tanaka, Y., Hishinuma, M., Nomoto, T., Maeda, T., Takubo, K., Suda, T. et al. (2014). R-spondins/Lgrs expression in tooth development. *Dev. Dyn.* **243**, 844-851. doi:10.1002/dvdy.24124

Kus-Bartoszek, A., Lipski, M., Jarzä…Bek, A., Manowiec, J. and Droździk, A. (2022). Gingival phenotype changes and the prevalence of mucogingival deformities during the early transitional dentition phase—a two-year longitudinal study. *Int. J. Environ. Res. Public Health* **19**, 3899. doi:10.3390/ijerph19073899

Lee, C. S., Buttitta, L. and Fan, C. M. (2001a). Evidence that the WNT-inducible growth arrest-specific gene 1 encodes an antagonist of sonic hedgehog signaling in the somite. *Proc. Natl. Acad. Sci. U.S.A.* **98**, 11347-11352. doi:10.1073/pnas.201418298

Lee, C. S., May, N. R. and Fan, C. M. (2001b). Transdifferentiation of the ventral retinal pigmented epithelium to neural retina in the growth arrest specific gene 1 mutant. *Dev. Biol.* **236**, 17-29. doi:10.1006/dbio.2001.0280

Li, J., Chatzeli, L., Panousopoulou, E., Tucker, A. S. and Green, J. B. A. (2016). Epithelial stratification and placode invagination are separable functions in early morphogenesis of the molar tooth. *Development (Camb.)* **143**, 670-681. doi:10.1242/dev.130187

Martinelli, D. C. and Fan, C. M. (2007). Gas1 extends the range of Hedgehog action by facilitating its signaling. *Genes Dev.* **21**, 1231-1243. doi:10.1101/gad.1546307

Miletich, I., Yu, W.-Y., Zhang, R., Sharpe, P. T., Caixeta De Andrade, S., Pereira, S. F. A., Ohazama, A., Mock, O. B., Buchner, G., Sealby, J. et al. (2011). Developmental stalling and organ-autonomous regulation of morphogenesis. *Proc. Natl. Acad. Sci. USA* **108**, 19270-19275. doi:10.1073/pnas.1112801108

Okada, A., Charron, F., Morin, S., Shin, D. S., Wong, K., Fabre, P. J., Tessier-Lavigne, M. and Mcconnell, S. K. (2006). Boc is a receptor for sonic hedgehog in the guidance of commissural axons. *Nature* **444**, 369-373. doi:10.1038/nature05246

Pavlikova, H., Witter, K. and Misek, I. (1999). Primordium of the upper vestibulum oris in the domestic sheep. *Acta Veterinaria Brno* **68**, 175-178. doi:10.2754/avb199968030175

Penon-Portmann, M., Eldomery, M. K., Potocki, L., Marafi, D., Posey, J. E., Coban-Akdemir, Z., Harel, T., Grochowski, C. M., Loucks, H., Devine, W. P. et al. (2022). De novo heterozygous variants in SLC30A7 are a candidate cause for Joubert syndrome. *Am. J. Med. Genet. A* **188**, 2360-2366. doi:10.1002/ajmg.a.62872

Peterková, R. (1985). The common developmental origin and phylogenetic aspects of teeth, rugae palatinae, and fornix vestibuli oris in the mouse. *J. Craniofac. Genet. Dev. Biol.* **5**, 89-104.

Placek, M., Mskach, M. and Mrklas, L. (1974). Significance of the labial frenum attachment in periodontal disease in man. Part 1. Classification and epidemiology of the labial frenum attachment. *J. Periodontol.* **45**, 891-894. doi:10.1902/jop.1974.45.12.891

Popa, E. M., Buchtova, M. and Tucker, A. S. (2019). Revitalising the rudimentary replacement dentition in the mouse. *Development* **146**, dev171363. doi:10.1242/dev.171363

Qiu, T. and Tucker, A. S. (2022). Mechanisms driving vestibular lamina formation and opening in the mouse. *J. Anat.* **242**, 224-234. doi:10.1111/joa.13771

Qiu, T., Teshima, T. H. N., Hovorakova, M. and Tucker, A. S. (2020). Development of the vestibular lamina in human embryos: morphogenesis and vestibule formation. *Front. Physiol.* **11**, 753. doi:10.3389/fphys.2020.00753

Ruiz-Perez, V. L., Blair, H. J., Rodriguez-Andres, M. E., Blanco, M. J., Wilson, A., Liu, Y.-N., Miles, C., Peters, H. and Goodship, J. A. (2007). Evc is a positive mediator of Ihh-regulated bone growth that localises at the base of chondrocyte cilia. *Development* **134**, 2903-2912. doi:10.1242/dev.007542

Sanz-Navarro, M., Delgado, I., Torres, M., Mustonen, T., Michon, F. and Rice, D. P. (2019). Dental epithelial sem cells express he developmental regulator Meis1. *Front. Physiol.* **10**, 249. doi:10.3389/phys.2019.00249

Sarkar, L., Cobourne, M., Naylor, S. and Sharpe, P. T. (2000). Wnt/Shh interactions regulate ectodermal boundary formation during mammalian tooth development. *Proc. Natl. Acad. Sci. USA* **97**, 4520-4524. doi:10.1073/pnas.97.9.4520

Sasalawad, S. S., Hugar, S. M., Poonacha, K. S. and Mallikarjuna, R. (2013). Ellis-van Creveld syndrome. *BMJ Case Rep.* **2013**, bcr2013009463. doi:10.1136/bcr-2013-009463

Schour, I. (1929). Early human tooth development, with special reference to the relationship between the dental lamina and the lip-furrow band. *J. Dent. Res.* **9**, 699-717. doi:10.1177/00220345290090050801

Seppala, M., Depew, M. J., Martinelli, D. C., Fan, C.-M., Sharpe, P. T. and Cobourne, M. T. (2007). Gas1 is a modifier for holoprosencephaly and genetically interacts with sonic hedgehog. *J. Clin. Investig.* **117**, 1575-1584. doi:10.1172/JCI32032

Seppala, M., Xavier, G. M., Fan, C.-M. and Cobourne, M. T. (2014). Boc modifies the spectrum of holoprosencephaly in the absence of Gas1 function. *Biology Open* **3**, 728-740. doi:10.1242/bio.20147989

Seppala, M., Fraser, G., Birjandi, A., Xavier, G. and Cobourne, M. (2017). Sonic hedgehog signaling and development of the dentition. *Journal of Developmental Biology* **5**, 6. doi:10.3390/jdb5020006

Seppala, M., Thivichon-Prince, B., Xavier, G. M., Shaffie, N., Sangani, I., Birjandi, A. A., Rooney, J., Lau, J. N. S., Dhaliwal, R., Rossi, O. et al. (2022). Gas1 regulates patterning of the murine and human dentitions through sonic hedgehog. *J. Dent. Res.* **101**, 473-482. doi:10.1177/00220345211049403

Soukup, V., Tazaki, A., Yamazaki, Y., Pospisilova, A., Epperlein, H.-H., Tanaka, E. M. and Cerny, R. (2021). Oral and palatal dentition of axolotl arises from a common tooth-competent zone along the ecto-endodermal boundary. *Front. Cell Dev. Biol.* **8**, 622308. doi:10.3389/fcell.2020.622308

Tenzen, T., Allen, B. L., Cole, F., Kang, J.-S., Krauss, R. S. and Mcmahon, A. P. (2006). The cell surface membrane proteins cdo and boc are components and targets of the hedgehog signaling pathway and feedback network in mice. *Dev. Cell* **10**, 647-656. doi:10.1016/j.devcel.2006.04.004

Tucker, A. S. (2010). Salivary gland adaptations: modification of the glands for novel uses. In *Salivary Glands*, pp. 21-31. Basel: Karger.

Tucker, A. S., Qiu, T., Buchtová, M. and Hovořáková, M. (2023). Transcriptional profiles (RNA-seq) of incisor tooth germ and adjacent vestibular lamina of E14 murine embryos. *FaceBase Consortium* doi:10.25550/2T-8JMG

Visel, A., Thaller, C. and Eichele, G. (2004). GenePain.org: an atlas of gene expression paterns in the mouse embryo. *Nuclie Acids Res.* **32**, D552-D556. doi:10.1093/nar/gkh029

Vonk, F. J., Admiraal, J. F., Jackson, K., Reshef, R., De Bakker, M. A. G., Vanderschoot, K., Van Den Berge, I., Van Atten, M., Burgerhout, E., Beck, A. et al. (2008). Evolutionary origin and development of snake fangs. *Nature* **454**, 630-633. doi:10.1038/nature07178

Wang, X. P., O'connell, D. J., Lund, J. J., Saadi, I., Kuraguchi, M., Turbe-Doan, A., Cavallesco, R., Kim, H., Park, P. J., Harada, H. et al. (2009). Apc inhibition of Wnt signaling regulates supernumerary tooth formation during embryogenesis and throughout adulthood. *Development* **136**, 1939-1949. doi:10.1242/dev.033803

Wilkinson, D. G. (1992). *In Situ Hybridisation: A Practical Approach*. Oxford: IRL Press.

Witter, K., Pavlikova, H., Matulova, P. and Misek, I. (2005). Relationship between vestibular lamina, dental lamina, and the developing oral vestibule in the upper jaw of the field vole (Microtus agrestis, Rodentia). *J. Morphol.* **265**, 264-270. doi:10.1002/jmor.10356

Xavier, G. M., Sharpe, P. T. and Cobourne, M. T. (2009). Scube1 is expressed during facial development in the mouse. *J. Exp. Zool. B Mol. Dev. Evol.* **312**, 518-524. doi:10.1002/jez.b.21260

Yu, W., Sun, Z., Sweat, Y., Sweat, M., Venugopalan, S. R., Eliason, S., Cao, H., Paine, M. L. and Amendt, B. A. (2020). Pitx2-Sox2-Lef1 interactions specify progenitor oral/dental epithelial cell signaling centers. *Development (Camb.)* **147**, dev186023. doi:10.1242/DEV.186023

Zhao, Z., Stock, D. W., Buchanan, A. V. and Weiss, K. M. (2000). Expression of Dlx genes during the development of the murine dentition. *Dev. Genes Evol.* **210**, 270-275. doi:10.1007/s004270050314